Traffic 2006; 7: 22–38
Blackwell Munksgaard

doi: 10.1111/j.1600-0854.2005.00356.x

Function and Mechanism of Action of *Dictyostelium* Nramp1 (Slc11a1) in Bacterial Infection

Barbara Peracino[1], Carina Wagner[2], Alessandra Balest[1], Alessandra Balbo[1], Barbara Pergolizzi[1], Angelika A. Noegel[3], Michael Steinert[2] and Salvatore Bozzaro[1,*]

[1]*Department of Clinical and Biological Sciences, University of Turin, Ospedale S. Luigi, 10043 Orbassano, Italy*
[2]*Institute for Molecular Infection-Biology, University of Würzburg, Röntgenring 11, 97070 Würzburg, Germany*
[3]*Center for Biochemistry, University of Cologne, Joseph-Stelzmann-Str. 52, 50931-Cologne, Germany*
** Corresponding author: Salvatore Bozzaro, salvatore.bozzaro@unito.it*

Dictyostelium **amoebae are professional phagocytes, which ingest bacteria as the principal source of food. We have cloned the *Dictyostelium* homologue of human natural resistance-associated membrane protein 1 (Nramp1) [solute carrier family 11 member 1 (Slc11a1)], an endo-lysosomal membrane protein that confers on macrophages resistance to infection by a variety of intracellular bacteria and protozoa. The *Dictyostelium Nramp1* gene encodes a protein of 53 kDa with 11 putative transmembrane domains. The *Nramp1* gene is transcribed during the growth-phase and downregulated to barely detectable levels upon starvation. To gain insights into their intracellular localization, we fused Nramp1 or the vatB subunit of the V-H$^+$ATPase with green fluorescent protein and expressed in cells. Green fluorescent protein-vatB was inserted in membranes of all acidic compartments and the contractile vacuole network and decorated macropinosomes and phagosomes. Green fluorescent protein-Nramp1 decorated macropinosomes and phagosomes, in addition to intracellular vesicular compartments positive for endosomal SNARE protein Vti1 or vacuolin, a marker of the exocytic pathway. *Nramp1* disruption generated mutants that were more permissive hosts than wild-type cells for intracellular growth of *Legionella pneumophila* and *Micobacterium avium*. *Nramp1* overexpression protected cells from *L. pneumophila* infection. Evidence is provided that Nramp1 transports metal cations out of the phagolysosome in an ATP-dependent process and that *L. pneumophila* and *M. avium* use different mechanisms to neutralize Nramp1 activity.**

Key words: *Dictyostelium*, endocytosis, host–pathogen interactions, iron transport, *Legionella*, *Micobacterium*, Nramp1, phagocytosis, V-H$^+$ATPase

Received 26 April 2005; revised and accepted 15 September 2005, published on-line 9 November 2005

Dictyostelium cells are an excellent experimental system to study phagocytosis (1–3). During their growth phase, the cells feed on bacteria, which are the primary source of food. The dynamics of phagocytosis is very similar in *Dictyostelium* and macrophages; in both the cases, particle adhesion to the cell surface induces local polymerization of the actin cytoskeleton, leading to pseudopodia extension, formation of phagocytic cups and phagosomes (1,4–6). The actin coat around the phagosome disappears in less than 2 min after ingestion (5,7), and the phagosome undergoes fusion with the endo-lysosomal compartment (8,9). Phagocytosis in *Dictyostelium* is regulated by heterotrimeric G-protein-linked signal transduction (5). In macrophages, the major regulatory network involves cytosolic tyrosine kinases of the *syk* family, which are linked to the Fcγ receptor (10). In both the systems, monomeric G proteins act as downstream effectors to the actin cytoskeleton (3,6). Components of the phagosome-lysosome fusing machinery or lysosomal enzymes and markers are also conserved in *Dictyostelium* and macrophages, confirming the ancient evolutionary origin of the phago-lysosomal apparatus (6,11,12). *Dictyostelium* cells are easily amenable to molecular genetic manipulation, such as generation of null or overexpressing mutants. In addition, the *Dictyostelium* genome has been fully sequenced (13,14), opening a variety of new approaches based on DNA arrays and proteomics to study phagocytosis. In this context, it was of interest to see whether *Dictyostelium* cells possess genes belonging to the natural resistance-associated membrane protein 1 (*Nramp1*) family.

Nramp1 was identified by positional cloning in the mouse *Bcg/Ity/Lsh* locus, which controls resistance to infections by *Mycobacteria, Salmonella* and *Leishmania* (15–17). The mammalian Nramp1 is expressed in the lysosomal membrane of mature macrophages, granulocytes and monocytes (18). Susceptibility to infections by intracellular parasites in inbred mouse strains is associated with a single point mutation in TM4 of the protein, which affects protein targeting, resulting in its accumulation in the endoplasmic reticulum (19). A human homologue of mouse Nramp1 is localized in the long arm of chromosome 2, polymorphic variants of which have been associated with susceptibility to tuberculosis and leprosy as well as autoimmune diseases (17,20).

The mechanism of action of Nramp1 is still debated (21). The protein belongs to a large family of metal ion transporters, including also Nramp2, a serpentine plasma membrane glycoprotein that transports several metal ions, in particular iron, manganese and zinc, into the cytoplasm (22–24). Ectopic expression of Nramp1 in COS cells (25) and *in vivo* measurements with metal-sensitive

fluorescent probes (26) have led to the proposal that Nramp1 acts as a symporter for protons and divalent metal ions out of the lysosome (17). According to this hypothesis, Nramp1 contributes to pH homeostasis while depleting the lysosomal milieu from metal ions that are required by several intracellular pathogens to activate their virulence genes. This notion has been questioned by other experiments with purified phagosomes, which suggest that Nramp1 acts instead as H^+/Fe^{++} anti-porter pumping ferric ions into the lysosome, thus contributing to production of oxygen radicals that would kill intracellular parasites (27–29). Other experiments suggest that Nramp1 influences the pattern of vacuolar fusion in the endocytic pathway (30–32). Any hypothesis on Nramp1 function in resistance to microbial infection has to take into account that many intracellular pathogens, such as *Mycobacteria* or *Legionella*, manipulate the endo-lysosomal pathway. It is therefore of importance to determine the exact intracellular location of the protein and its fate during pathogen infection.

Microbes pathogenic for *Dictyostelium* have been described long ago (33). Recent studies have shown that *Dictyostelium* cells can be used as a model system for studying infections by *Mycobacteria* (34) and *Legionella pneumophila* (35–38). *Micobacterium avium* causes bacteremia, disseminated multiorgan bacterial disease and pulmonary infections. *Legionella pneumophila* is known to be the causative agent of a severe pneumonia. The manipulation of the *Nramp1* gene within *Dictyostelium* allows the function of the corresponding protein to be analysed during bacterial infection. This approach may also help in elucidating the exact role of Nramp1 in human macrophages.

In this article, we describe the cloning of the *Dictyostelium Nramp1* gene and its expression during development. By generating green fluorescent protein (GFP)-fusion proteins with Nramp1 and the vatB subunit of the V-H^+ATPase, a marker of the endo-lysosomal pathway (39), we have examined the intracellular localization of both proteins and their recruitment in pino- and phagosomes. We have generated *Nramp1* null and overexpressing strains to study Nramp1 function in bacterial infection and provide new evidence on the metal-transport properties of the protein.

Results

Cloning, characterization and transcriptional regulation of Dictyostelium Nramp1 gene

The consensus transport signature of the *Nramp1* gene family, in addition to the *trans*-membrane domains (TM), is highly conserved from bacteria to humans (40). This region and a sequence downstream of the third TM of human Nramp1 were chosen to construct two degenerated primers that were assayed on genomic DNA extracted from growth-phase AX2 cells. A 619-bp fragment, highly homologous to the expected central region of the gene, was amplified, and its sequence information used to search for contiguous sequences in the genomic library assembled by the *Dictyostelium* genome project (http://www.dictybase.org). Using the information derived from the genomic library and by designing appropriate primers, we progressively cloned and sequenced the entire gene. The final clone consists of a 1695 bp sequence, which encodes an open-reading frame of 1602 bp starting at the ATG in position +8 with a 111 bp intron from nucleotide +199 to nucleotide +309. Generating and sequencing a cDNA confirmed the genomic DNA sequence and the position of the intron.

The deduced amino acid sequence shows 55% homology to human Nramp1 and Nramp2 (Figure 1). The highest degree of sequence conservation is found in the transmembrane domains (about 70% homology) and in the consensus-transport signature (90% homology) (Figure 1). The highest variability is at the hydrophilic N- and C-terminal sequences, as usual in the Nramp family (40). *Dictyostelium Nramp1* encodes a protein of 53 kDa, with 11 putative TM domains (TM8 of human and murine Nramp1 being absent in the *Dictyostelium* homologue), with the conserved intracytoplasmic consensus-transport signature (40), but no putative N glycosylation sites. On the basis of sequence analysis by distance matrix to determine the relative branching of *Dictyostelium* from the line leading to humans, *Dictyostelium discoideum* Nramp1 is closer to humans than the yeast and *Arabidopsis* Nramp homologues (data not shown). This confirms the hypothesis that *Dictyostelium* diverged much later than plants and yeast (41,42).

A genomic DNA pattern was generated with five restriction enzymes and hybridized with either the 1350 bp fragment downstream of the intron or the 619 bp probe corresponding to the central core of the protein, containing the consensus-transport signature. An identical pattern was obtained with both the probes, which is consistent with the *Nramp1* gene being present in single copy (data not shown).

Northern blot analysis of total RNA extracted from axenically growing cells or cells at different developmental times showed that the *Nramp1* gene is expressed during growth (t_0). Expression declines rapidly upon starvation, and the mRNA is barely detectable in cells developed for 2 or more hours (Figure 2).

Intracellular pattern of Nramp1(C)-GFP and GFP-(N)vatB in resting cells, macropinocytosis and phagocytosis

The distribution of Nramp1 in living cells was studied by generating a cell line expressing a GFP-fusion protein under the control of a constitutive actin promoter. As the protein was expected to label the endo-lysosomal

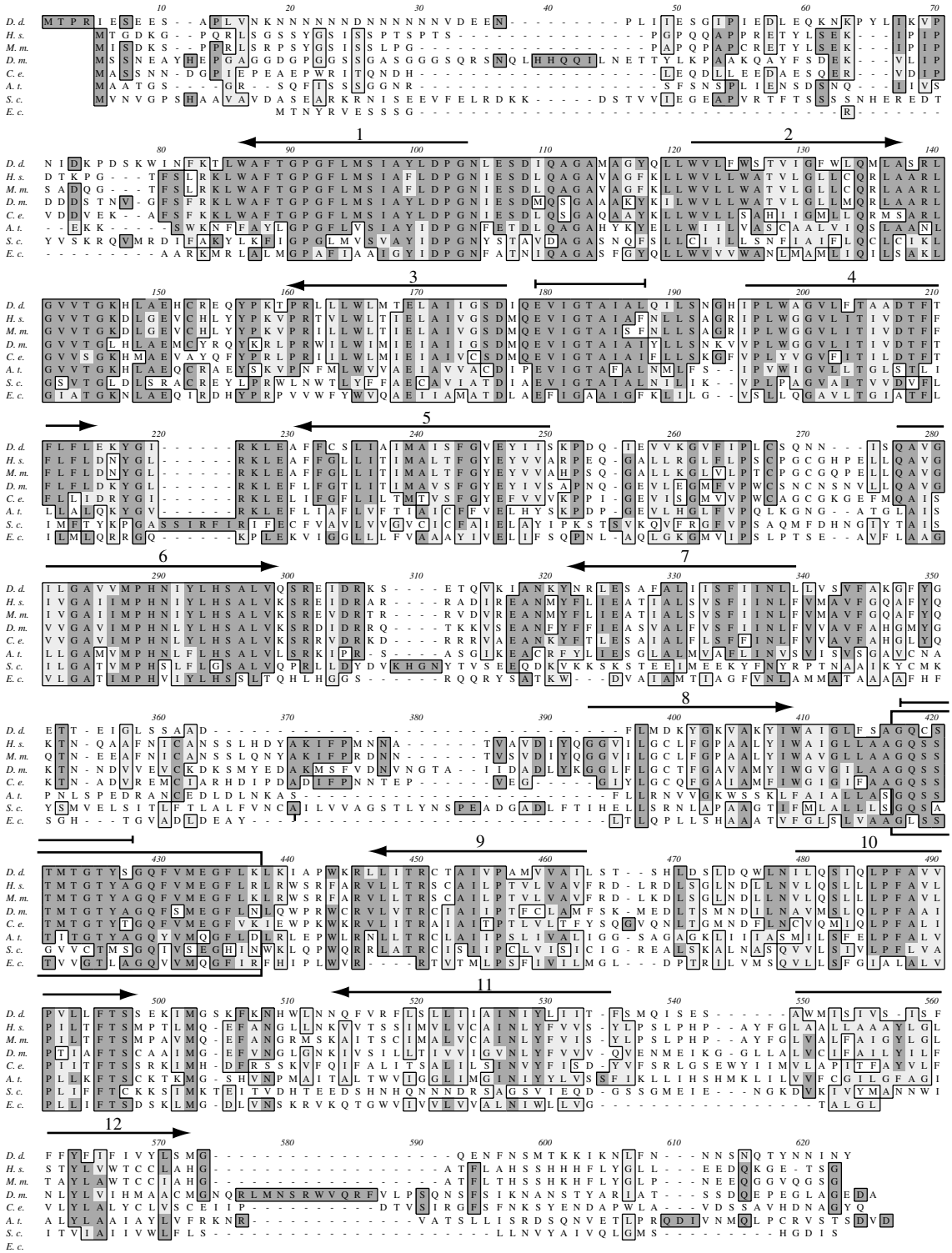

Figure 1: Amino acid sequence of *Dictyostelium* Nramp1 and alignment with other Nramp1-related polypeptides. The *Nramp1* sequences from *D. discoideum* (*D. d.*), *H. sapiens* (*H. s.*, NCBI accession no. BAA08907), *M. musculus* (*M. m.*, Swiss Prot. no. P41251), *D. melanogaster* (*D. m.*, AAL13772), *C. elegans* (*C. e.*, NP_509132), *A. thaliana* (*A. t.*, NP_178198), *S. ceverisiae* (*S. c.*, NP_014519) and *E. coli* (*E. c.*, NP_311298) were aligned using the MacVector Clustal W program (Blosum matrix). Residues identical in at least five sequences are shown in dark grey and homologous residues in light grey. Arrows indicate the putative transmembrane domains, with their relative orientation, in human and murine Nramp1; notice that TM8 is absent in *D. d.* Nramp1. The conserved transport signature is framed, and the two sequences used to generate the primers for the initial cloning of *D. d.* Nramp1 are indicated with segments. *D. d. Nramp1* sequence can be accessed under the number DDB0202615 (http://www.dictybase.org).

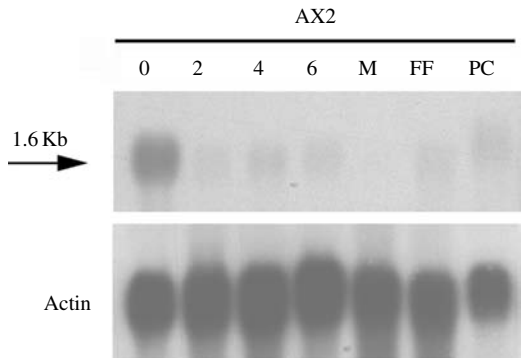

Figure 2: Expression of the *Nramp1* gene during *Dictyostelium* development. Total RNA was prepared from cells shaken in suspension for the time (in hours) indicated on top or from cells plated on filter and harvested at the stages indicated (M, mounds; FF, first finger and PC, preculminants). RNA extraction, electrophoresis and blotting were done as described in *Materials and Methods*. The blot was hybridized with a ^{32}P-labelled DNA fragment of 1350 bp, corresponding to the amino acid region 84–533. To quantify the relative RNA amount in each lane, we also hybridized the blot with a DNA fragment encoding actin (bottom).

compartment, cells expressing a GFP fused to the vatB subunit of the vacuolar H^+ATPase (39) were also generated and examined in parallel. Co-localization of both the proteins was also tested, using an antibody against the vatA subunit of the V-H^+ATPase in immunofluorescence experiments.

In resting cells, Nramp1(C)-GFP is located at the periphery of vesicles of variable size, which are distributed all over the cytoplasm, in part clustered at a perinuclear site. The protein is absent from the cell surface or the nucleus (Figure 3A, top). The perinuclear cluster is present in all cells that we have examined, independent of fluorescence intensity. Careful examination at the confocal fluorescence microscope showed that several tiny vesicles travel rapidly outward from and towards the perinuclear cluster (not shown). Evidence will be presented further below that this cluster is identical with the *trans*-Golgi network (TGN).

Nramp1(C)-GFP is not detected in the contractile vacuole system, an osmoregulatory organelle in which the vacuolar H^+ATPase is enriched (43,44). Figure 3A, bottom, shows progressive confocal sections of a cell expressing the GFP-(N)vatB subunit. The contractile vacuole appears as a convoluted bladder and duct network located at the bottom of the cell in contact with the substratum. Other vesicles decorated with GFP-(N)vatB but not connected to the network are also visible, and their number increases in upper confocal sections of the cell (Figure 3A). As shown below, these vesicles are part of the endo- and phagolysosomal pathway. The morphology of the GFP-(N)vatB-labelled contractile vacuole network is remarkably similar to that described with GFP-dajumin, a rather specific marker of the vacuole network that does not decorate endosomal vesicles (45).

Immunofluorescence staining with anti-vatA antibody shows full coincidence between vatA and GFP-(N)vatB fluorescence, both in the contractile vacuole network and in isolated vesicles dispersed all over the cell (Figure 3B, right). In contrast, few vatA-positive vesicles are decorated with Nramp1(C)-GFP, mostly smaller ones, some of which are scattered in the perinuclear cluster (Figure 3B, left). Consistent with the *in vivo* distribution of GFP-Nramp1 (Figure 3A, top), the GFP-fused protein fails to co-localize with the vatA-decorated contractile vacuole network (Figure 3B, left).

The intracellular patterns of Nramp1(C)-GFP and the vacuolar H^+ATPase in resting cells thus differ in several respects: a minority of vesicles are decorated with both proteins, the V-H^+ATPase [as detected with both GFP-(N)vatB and anti-vatA] is massively present in the contractile vacuole network, whereas Nramp1(C)-GFP is enriched in a perinuclear cluster.

In terms of position and shape, the perinuclear cluster is strikingly similar to the Golgi stacks, as detected in *Dictyostelium* cells expressing the Golgi marker GFP-golvesin (46). To confirm its identity with the Golgi, cells-expressing Nramp1(C)-GFP were permeabilized and incubated with an antibody specific for the Golgi-associated protein comitin (47). As shown in Figure 4, the anti-comitin antibody strongly labelled the core of the cluster decorated with Nramp1(C)-GFP.

The permeabilized cells were also co-labelled with antibodies against Vti1 and vacuolin. Vacuolin is enriched in vesicles of the postlysosomal pathway (7,48), whereas Vti1 is a component of a Qb-SNARE complex involved in multiple vesicle transport and targeting from the TGN to the early endosomes or lysosomes (49–51). Vti1 decorated most, if not all, vesicles coated with Nramp1(C)-GFP but very few expressing GFP-(N)vatB. Remarkably, Vti1 labelled the perinuclear cluster defined by Nramp1(C)-GFP, similar to comitin (Figure 4). Co-localization with Vti1 suggests that the perinuclear cluster very likely represents the TGN and vesicles budding from it. The very high co-localization between Vti1 and Nramp1(C)-GFP also in vesicles outside the Golgi suggest that Nramp1 is inserted with Vti1 in the same vesicles and the Vti1 SNARE complex regulates its transport and docking along the endosomal pathway.

Vacuolin co-localized with some Nramp1(C)-GFP-decorated vesicles but few if any vesicles decorated with GFP-(N)vatB (Figure 4). These results are consistent with the notion that vacuolin is mainly expressed in non-acidic, postlysosomal vesicles (48) and suggest that Nramp1 might detect an intermediate step in the postlysosomal pathway.

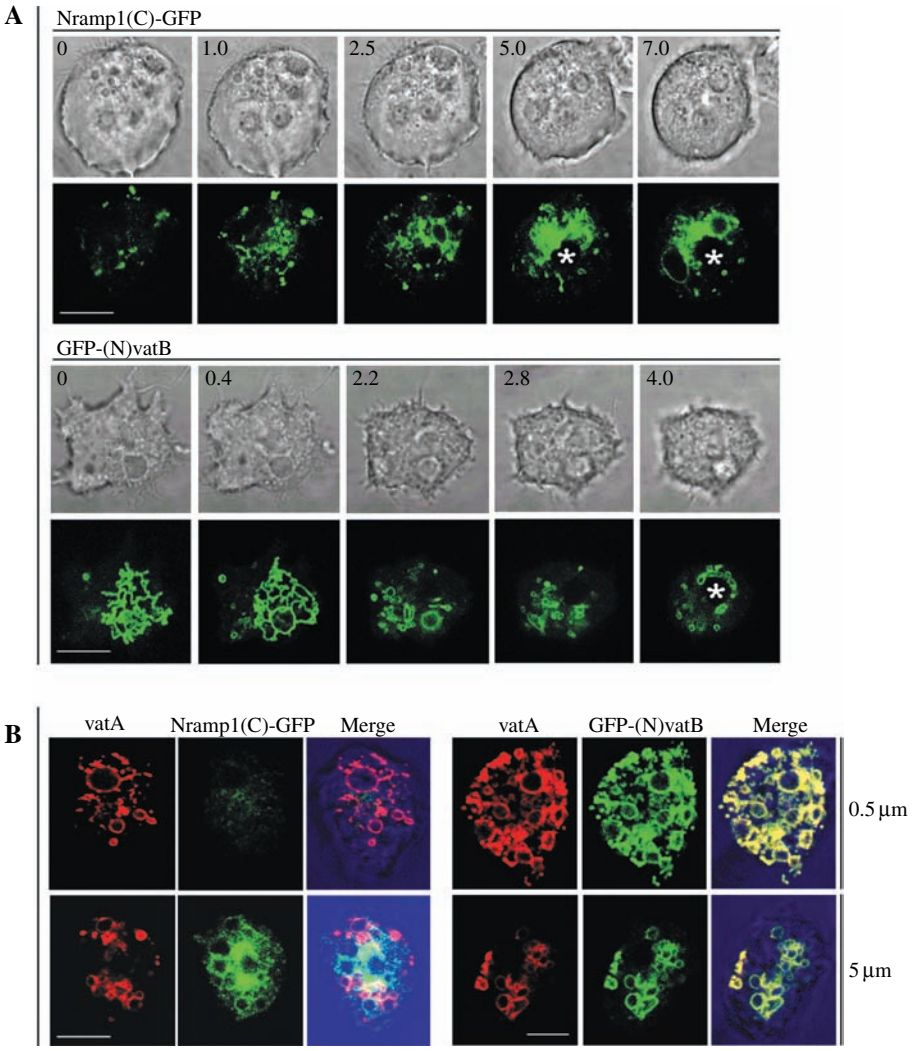

Figure 3: Dynamics of Nramp1 and vacuolar H^+-ATPase vatB subunit in living cells visualized by GFP fusion proteins and co-localization with vatA. (A) Confocal phase-contrast and corresponding GFP fluorescence sections through living cells expressing Nramp1(C)-GFP or GFP-(N)vatB. The numbers indicate distance in μm from the bottom surface of the cell. The contractile vacuole network, evidenced by the GFP-(N)vatB decoration, is typically localized in the bottom region of the cell close to the substratum (sections 0–0.4 μm). Note the absence of a similarly decorated structure in corresponding sections of Nramp1(C)-GFP-expressing cells. Nramp1(C)-GFP is distributed in small vesicles and clustered in part adjacent to the nucleus. The perinuclear distribution of Nramp1(C)-GFP is evident in the upper section stack (A, sections 5–7 μm), where the nucleus is marked by an asterisk. (B) VatA distribution in AX2 cells expressing the GFP fusion proteins. The cells were plated on glass coverslip, permeabilized with cold methanol and incubated with anti-vatA antibodies. Binding was detected with TRITC-labelled anti-mouse IgG. Confocal stacks of two cells are shown. The contractile vacuole network is labelled with vatA and GFP-(N)vatB, not Nramp1(C)-GFP (section 0.5 μm). Note total superimposition of red and green fluorescence for vatA and GFP-(N)vatB (right) and partial one for vatA and Nramp1(C)-GFP. Little coincidence is found for the last two proteins also in the perinuclear cluster. Bars: 5 μm.

To study *in vivo* recruitment of Nramp1(C)-GFP or GFP-(N)vatB during macropinocytosis and phagocytosis, we incubated cells with either TRITC-dextran, a fluid-phase marker which is taken up by macropinocytosis (52), or heat-killed yeast particles, which undergo phagocytosis (1,5). TRITC-dextran-filled vesicles underwent fusion with Nramp1(C)-GFP-decorated vesicles after a lag of 95 seconds at the earliest from macropinosome formation (Figure 5, left). In pulse-chase experiments, after 5-min chase, all TRITC-dextran-loaded vesicles were decorated with GFP-(N)vatB but only 25% with Nramp1(C)-GFP (Figure 5, right). At later time points, the number of vatB-labelled TRITC-dextran vesicles decreased, while Nramp1-labelled vesicles increased (Figure 5, right). Thus, it appears that macropinosomes fuse first with GFP-(N)vatB, and shortly thereafter with Nramp1(C)-GFP-decorated vesicles. These results confirm previous findings that the V-H^+ATPase is recruited very early following endosome formation (53).

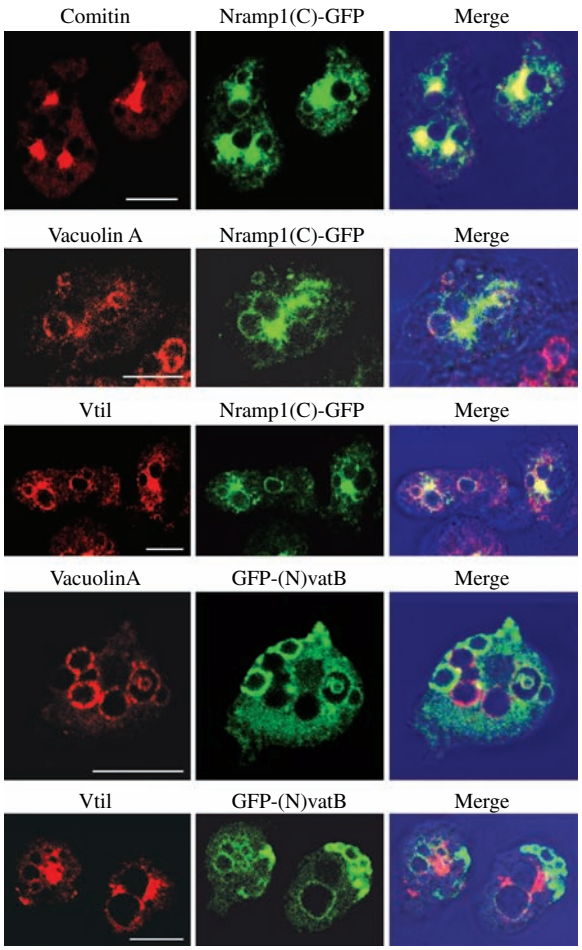

Figure 4: Co-localization of GFP fusion proteins with comitin, vacuolin and Vti1. AX2 cells expressing Nramp1(C)-GFP or GFP-(N)vatB were plated on glass coverslips. They were fixed, permeabilized with cold methanol and incubated with monoclonal antibodies specific for the Golgi-associated protein comitin, the exocytic marker vacuolin or the SNARE protein Vti1. For immunolabelling, secondary TRITC-labelled IgG was used. The core of the perinuclear cluster, decorated with Nramp1(C)-GFP, costains with anti-comitin and anti-Vti1 antibodies. Most vesicles positive for Vti1 co-label with Nramp1 but not with vatB. Many vesicles decorated with vacuolin co-label with Nramp1(C)-GFP few if any with GFP-(N)vatB. Bars: 5 μm.

Ingested yeast particles or bacteria were found, within 15 min of incubation, in Nramp1(C)-GFP- or GFP-(N)vatB-labelled vesicles. Figure 6A shows two cells containing yeast particles in vesicles decorated with Nramp1(C)-GFP. Similar results are obtained with GFP-(N)vatB-expressing cells (not shown). Figure 6A (lower panel) exemplifies co-localization of vatA and Nramp1(C)-GFP in a yeast phagosome, indicating that both Nramp1 and the V-H^+ATPase are eventually recruited to engulfed phagosomes. Figure 6B illustrates that both non-pathogenic and pathogenic bacteria can be found, several minutes after ingestion, in Nramp1-positive phagosomes. We never observed Nramp1(C)-GFP or GFP-(N)vatB in phagocytic cups or around yeast particles just engulfed by the cell, suggesting that both the proteins are not required for uptake and phagosome formation. A statistically significant kinetic analysis of yeast particle trafficking over time was not possible, as the number of ingested particles, particularly with cells expressing GFP-(N)vatB, was very low and variable. Experiments are in progress to study the kinetics of phagocytosis with non-pathogenic and pathogenic bacteria as well as latex beads.

Co-localization of Nramp1(C)-GFP and GFP-(N)vatB with the acidic marker neutral red

Nramp1(C)-GFP- and GFP-(N)vatB-expressing cells were incubated with neutral red, a vital stain that becomes concentrated in autophagic and acidic vacuoles, and has been widely used in *Dictyostelium* as marker of lysosomes as well as other acidic vesicles. Figure 7 shows cells expressing the GFP chimaeras and incubated for 10 min with neutral red. In cells expressing GFP-(N)vatB, neutral red spots and GFP-(N)vatB fluorescence were fully superimposable, with the exception of the contractile vacuole network (Figure 7, right). This is consistent with the finding that the lumen of the contractile vacuole is not acidic, despite the high concentration of proton pumps in the membrane, and is not stained by neutral red (54). In contrast to GFP-(N)vatB, most, but not all, Nramp1(C)-GFP-decorated vesicles contain neutral red (Figure 7, left). Thus, GFP-(N)vatB appears to decorate all acidic vesicles in the cell, whereas Nramp1(C)-GFP is found in a subclass only of acidic vesicles in addition to non-acidic vesicles. Similar results were obtained with Lysotracker red, which however, in our hands was less specific for acidic vacuoles, as it also labelled the surface of the contractile vacuole network (data not shown).

Effects of Nramp1 gene disruption or overexpression on intracellular growth of L. pneumophila and M. avium

Nramp1-null mutants were generated by homologous recombination as described in *Materials and Methods*. Figure 8, left, shows the typical band shift in Southern blot of a clone (named HSB60) because of insertion of the blasticidin resistance (*bsr*) cassette within the *Nramp1* gene. As consequence, no band was expressed in correspondence to the *Nramp1* mRNA in Northern blots of the HSB60 cells (Figure 8, right). A lower band was detected by probing with a cDNA probe of 845 bp corresponding to the DNA region downstream of the intron and upstream of the *bsr* cassette (Figure 8A), suggesting that gene disruption leads to expression of a truncated form of *Nramp1* mRNA. It is unlikely that the truncated mRNA is stable and translated optimally because of the absence of a polyadenylation signal. Assuming it to undergo translation, the resulting polypeptide would consists of the first six TM domains only and would lack the consensus signature sequence, which is crucial for the activity of the protein (40). It is therefore likely that a truncated protein would be non-functional.

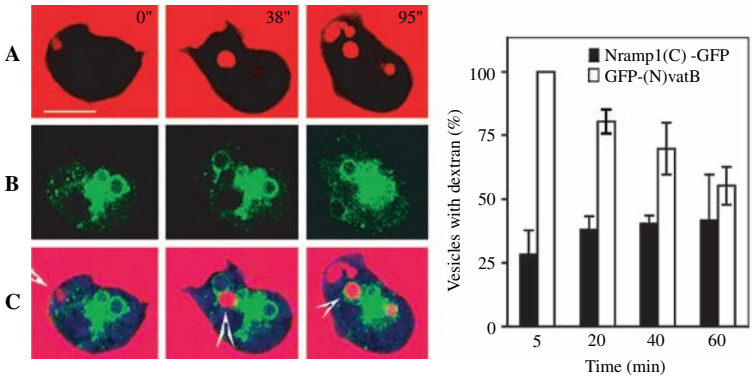

Figure 5: Recruitment of Nramp1(C)-GFP and GFP-(N)vatB in macropinosomes. (Left) Cells expressing Nramp1(C)-GFP were plated on glass coverslips and incubated with the fluid-phase tracer, TRITC-dextran. Confocal images were taken every 9.2 seconds. Consecutive images of a single cell are shown after ingestion of the fluid phase tracer (time: 0 seconds). (A) TRITC-dextran fluorescence, (B) GFP fluorescence and (C) superimposed red and green fluorescence with contrast phase images (blue). A GFP-uncoated TRITC-dextran-filled vesicle (time: 0 seconds, arrowhead) re-emerges in the centre of the cell and fuses with Nramp1(C)-GFP after 95 seconds (arrowhead). Note the formation of two endocytic cups in the upper part of the cell (38 seconds) that leads to ingestion of TRITC-dextran, forming three GFP-uncoated vesicles at time 95 seconds. (Right) Cells expressing the GFP fusion proteins were pulsed with TRITC-dextran for 5 min under shaking. Excess TRITC-dextran was washed out, and the cells were plated on glass coverslips. Confocal images were taken after 5–60 min of chase. The number of TRITC-dextran positive vesicles coated with either Nramp1(C)-GFP or GFP-(N)vatB is plotted over time. For each time point, an average of 50 macropinosomes and 15 cells per experiment were counted. Mean values of three independent experiments with SD (error bars) are shown. Bar: 5 μm.

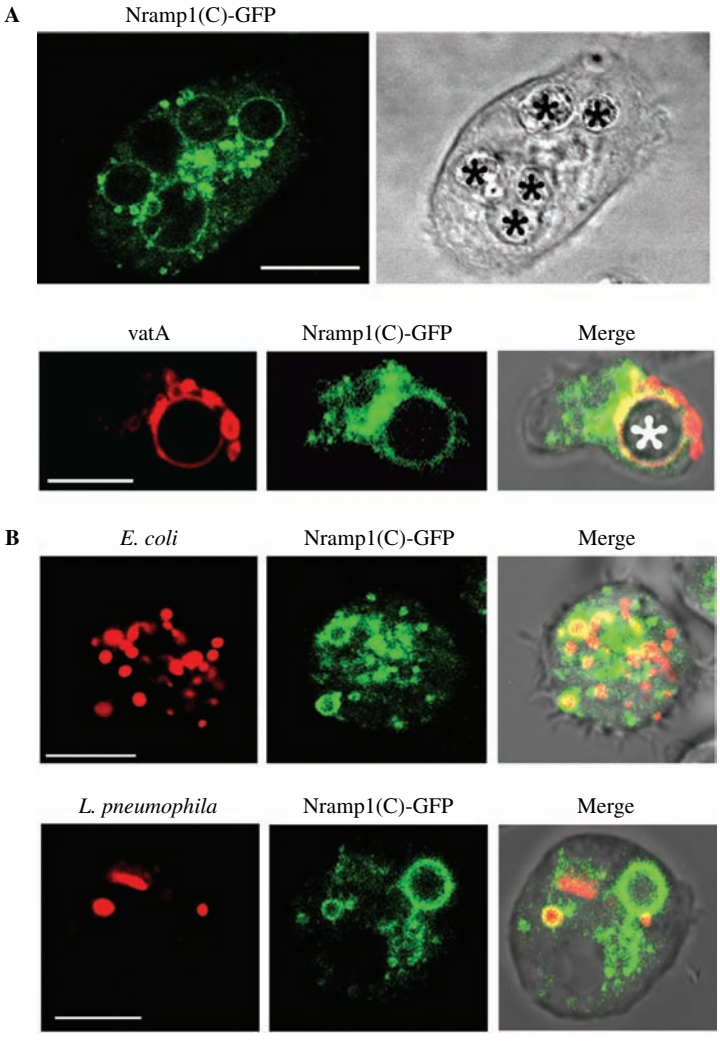

Figure 6: Localization of Nramp1(C)-GFP and vatA with phagosomes. (A) Living AX2 cells expressing the GFP chimaera were allowed to adhere to glass coverslips and incubated with heat-treated yeast particles. Confocal section images were taken after 15-min incubation. In parallel, cell samples were fixed and treated with anti-vatA antibodies. Fluorescence and corresponding contrast phase images are shown. Yeast particles within phagosomes are marked by an asterisk. (B) Living AX2 cells expressing the GFP fused protein were pulsed with TRITC-labelled *E. coli* or *L. pneumophila* for 15 min, washed and further incubated for 15 or 30 min, respectively. Note that *E. coli* are taken up much more avidly than *L. pneumophila*. In both the cases, some bacteria are decorated with Nramp1(C)-GFP. Bars: 5 μm.

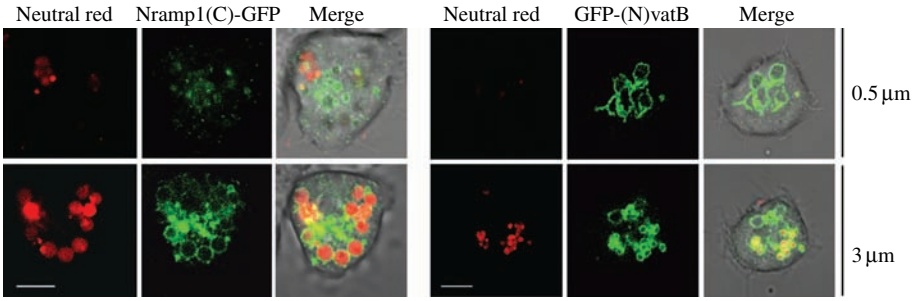

Figure 7: Co-localization of Nramp1(C)-GFP and GFP-(N)vatB with the acidic fluorescent marker neutral red. AX2 cells expressing the GFP fusion proteins were incubated with neutral red for 5 min, washed and allowed to adhere to a glass coverslip for 10 min before observation. Neutral red fluorescence, GFP fluorescence and superimposed red and green fluorescence with contrast phase are shown. Neutral red does not label the contractile vacuole network (section 0.5 μm), otherwise all neutral red spots are coated with GFP-(N)vatB but only some of them with Nramp1(C)-GFP. Bars: 5 μm.

HSB60 mutant cells displayed no defects in the rate of axenic growth or growth on *Escherichia coli* lawns. Cells underwent aggregation and fruiting body formation similar to the parental AX2 strain, except that postaggregative development was accelerated by a few hours.

We tested susceptibility to infection by pathogenic bacteria (*L. pneumophila* Corby or *M. avium*) in the mutant, using as control the AX2 parental strain and cells expressing *Nramp1* constitutively. As shown in Figure 9, the intracellular growth rate of *L. pneumophila* and *M. avium* were significantly higher in HSB60 cells when compared with AX2 cells. Remarkably, overexpressing *Nramp1* under the control of a constitutive promoter inhibited completely *L. pneumophila* not however *M. avium* growth (Figure 9). We attempted to rescue the knockout mutant by expressing *Nramp1(C)-GFP* under the control of a constitutive promoter. Two independent clones were assayed with *L. pneumophila.* Interestingly, *L. pneumophila* intracellular growth was inhibited similar to AX2 cells overexpressing *Nramp1* (Figure 9).

Effects of L. pneumophila and M. avium infection on Nramp1 gene expression

We have shown that the *Nramp1* gene is expressed during growth and repressed in starving cells (Figure 2). To test whether its expression is altered during infection with pathogenic bacteria, we incubated AX2 cells either in medium alone or with pathogenic *L. pneumophila* or *M. avium* strains. The medium is a half-starving medium, which does not allow cell or bacterial growth, but inhibits cell aggregation over the infection period (35,36). Total RNA was extracted every 24 h and subjected to electrophoresis and hybridization with the *Nramp1* probe. As a control, the Northern blots were also hybridized with *vatB* and *actin* DNA probes. Figure 10 shows a representative Northern blot and quantitative data of three separate experiments. Despite high variation in the error bars, a trend is detectable. In control cells incubated in medium alone, *Nramp1* RNA expression started to decrease at 48 h and was faintly detectable at 72 h of incubation. This pattern seems to reflect the inhibitory effect on

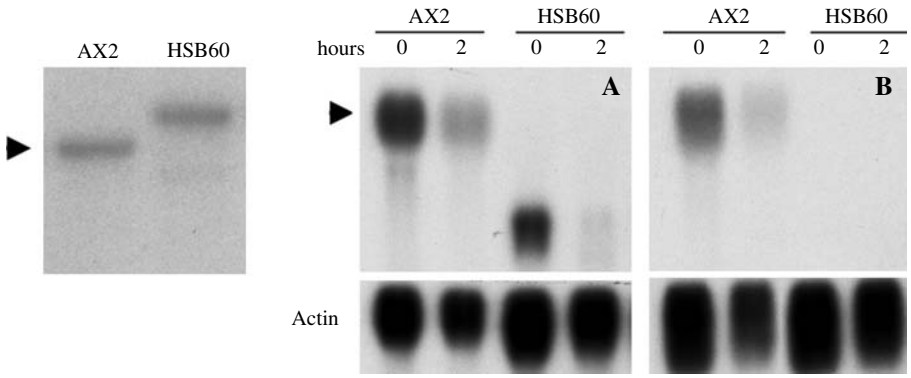

Figure 8: Nramp1 gene disruption in HSB60 cells. Mutant HSB60 was generated by homologous recombination of parental AX2 cells as described in *Materials and Methods*. DNA and total RNA were extracted from AX2 or HSB60 cells and subjected to (left) Southern or (right) Northern blot. The Southern blot was hybridized with a cDNA of 1390 bp, covering the region of the Nramp1 gene downstream of the intron. The Northern blot was hybridized with (A) cDNA probe I of 845 bp, covering the region +1/845, and (B) cDNA probe II, which covers the region +846/1593. A band shift because of insertion of the *bsr* cassette is evident in the Southern blot. In Northern blot, a lower band is labelled with DNA probe I, none with DNA probe II, indicating that a truncated mRNA is produced as a consequence of the *bsr* insertion.

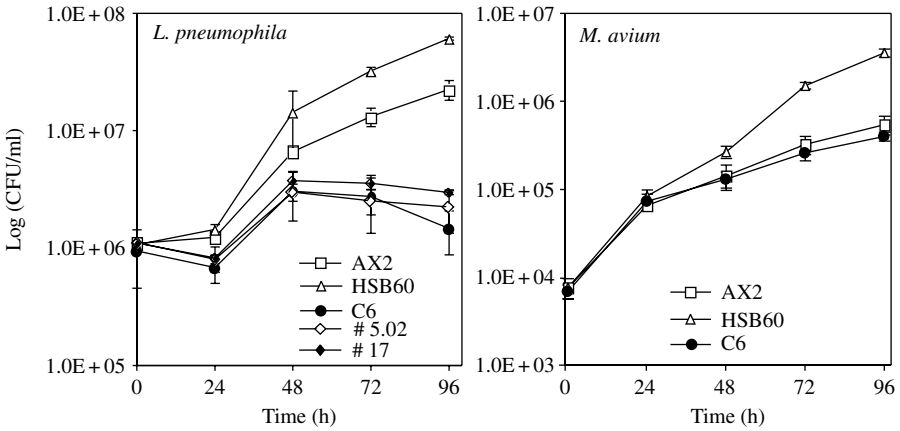

Figure 9: Effects of *Nramp1* gene disruption or overexpression on *L. pneumophila* and *M. avium* infectiveness. (Left) Cells were coincubated with 1×10^6/mL *L. pneumophila* (at a MOI 1:1) in a solution of MB medium (38) in 96-well plates at 24.5 °C. To favour infection, the plates were centrifuged at 700 × g. per 10 min (38). At the time indicated in the abscissa, adherent cells were removed from the culture flask and lysed by repeated pipetting. Bacterial colony forming units (cfu) were determined by plating 10-fold dilution series. The following cell lines were used: AX2, *Nramp1*-null mutant HSB60, AX2 cells overexpressing *Nramp1(C)-GFP* (clone C6) and HSB60 cells transfected with *Nramp1*(*C)-GFP* and selected with 20 μg/mL G418 (clones 5.02 and 17). (Right) For *M. avium* infection, the cells were co-incubated with 1×10^6 bacteria (at a MOI of 1:2) per millilitre. Three hours postinfection, extracellular bacteria were removed by washing. The remaining extracellular bacteria were killed by 30-min exposure to 0.2 mg amikacin/mL. Thereafter, the medium was replaced by medium containing 0.02 mg/mL amikacin (0 time point). At the indicated time intervals, the bacterial numbers (cfu) were determined by removing and lysing *Dictyostelium* cells and by plating 10-fold dilution series (39). The figure shows the mean values of three to six independent experiments, each done in triplicate ±SD (error bars) for *L. pneumophila* and one representative experiment, in triplicate ±SD, for *M. avium*. The experiments have been repeated several times with *L. pneumophila and* at least three times with *M. avium* with comparable results.

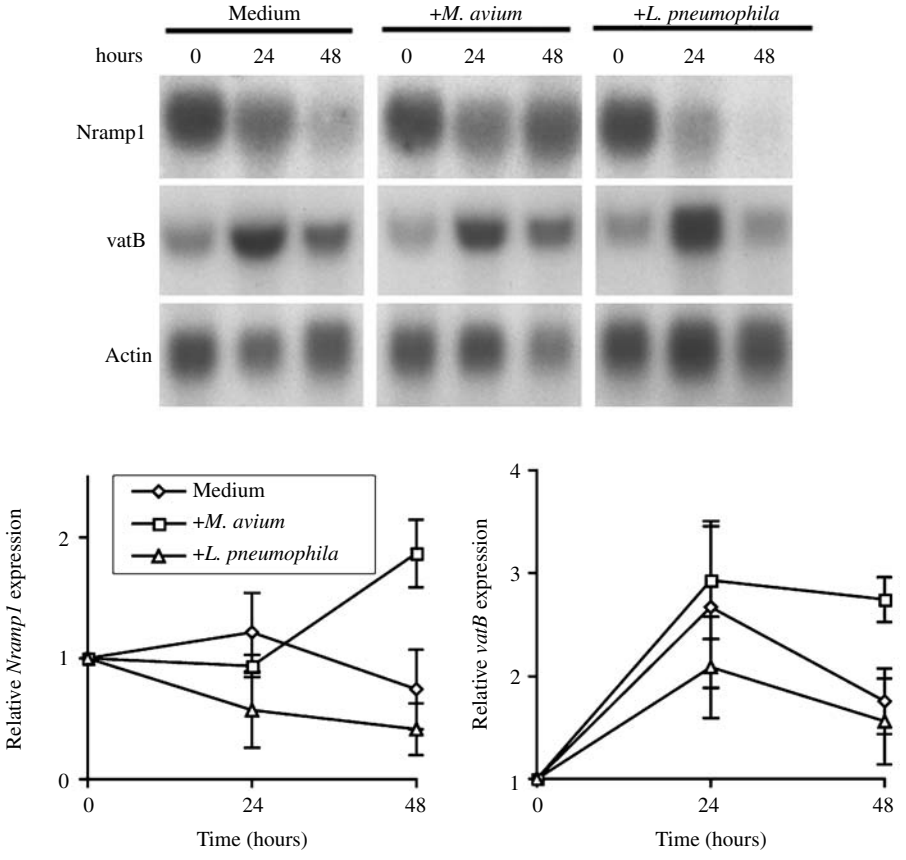

Figure 10: Effects of *L. pneumophila* or *M. avium* infection on Nramp1 gene expression. AX2 cells were incubated either in medium alone (1:1 HL5-medium and Soerensen phosphate buffer) or with *L. pneumophila* or *M. avium* as described in the legend to Figure 9 but at a MOI of 1:100. At the time points indicated, cells were withdrawn from the culture and RNA extracted with TRIzol. After electrophoresis and transfer to Hybond-N membranes, the Northern blots were hybridized with the DNA probes indicated on the left. Densimotetric quantification of Northern blots from three independent experiments were evaluated using the ImageJ 1.31v software. Mean values of *Nramp1* and *vatB* expression have been normalized for the corresponding loading control (actin) at each time point. They are expressed relative to the values at time 0 = 1.

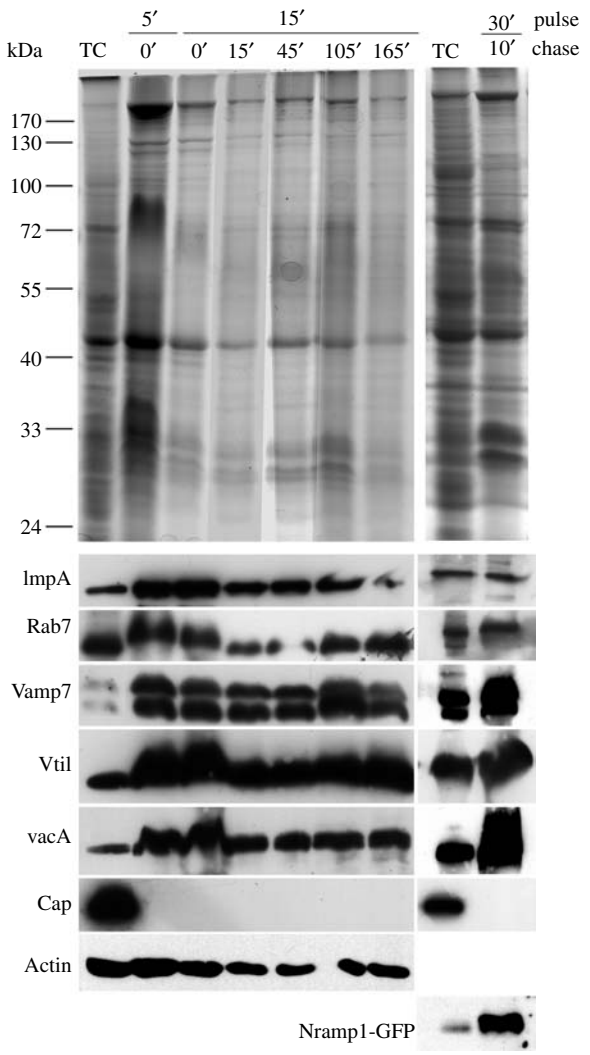

Figure 11: Characterization of purified phagosomes. Cells were incubated with fluorescent latex beads for either 5, 15 or 30 min, washed from unbound beads and chased in buffer for the time indicated (in min). Phagosomal fractions were purified as described in *Materials and Methods*. Total proteins from whole cells (TC) or purified phagosomes were subjected to SDS–PAGE, blotted onto nitrocellulose and immunolabelled with antibodies against the proteins listed on the left. The distribution pattern of β-Cop (not shown) was the same as Cap. (Upper panel) Coomassie Blue staining; (lower panel) immunoblots. For each electrophoresis lane, the same volume of each sample was used in different immunoblots to allow for internal comparison. Note, however, from the Coomassie Blue staining, that the total protein concentration appears to be higher in lanes 1 and 2. Phagosomal fractions similar to the 30/10 min samples shown on the right were used for the iron transport studies (Figure 12). The protein content in the last two right lanes was similar (not shown).

Nramp1 accumulation observed during starving conditions (Figure 2), except that the mRNA declines much more slowly, very likely because of the suboptimal nutritive properties of the medium. Remarkably opposite effects were observed during infection with *M. avium* or *L. pneumophila*. *Nramp1* RNA accumulation persisted, and even increased, over the 48 h of incubation in cells infected with *M. avium*, whereas it declined between 24 and 48 h of *L. pneumophila* infection more rapidly than in control cells left in medium (Figure 10). *Nramp1* RNA continued to accumulate at 72 h of infection with *M. avium* (data not shown). At this time point, results with *L. pneumophila* could not be evaluated because of some cell lysis and total degradation of extracted RNA in three separate experiments. The half-life of most proteins in *Dictyostelium* is 4 h; therefore, the drastic *Nramp1* RNA inhibition occurring between 24 and 48 h of Legionella infection very likely leads to rapid decrease and disappearance of the endogenous protein by 40–50 h of infection. A dramatic increase for *vatB* mRNA is evident at 24 h in all cases, followed by a decrease at 48 h, less pronounced for cells infected with *M. avium*. It is known that *vatB* expression is modulated by nutrients, being rapidly downregulated by washing in nutrient-free medium and upregulated upon cell transfer in axenic medium or non-pathogenic bacterial culture (39). Thus, we believe that upregulation at 24 h reflects cell transfer in a medium containing nutrients although unable to sustain cell growth. The decrease at 48 h could reflect a starvation effect as evidenced for *Nramp1*, but we have no explanation for the lower decrease observed in the presence of *M. avium*.

Effects of Nramp1 gene disruption or overexpression on iron transport across the phago-lysosomal membrane

It is well established that Nramp1 transports metal ions, particularly iron, manganese and zinc, but it is debated whether the ions are transported into or outside the lysosomal lumen (17,21). To test whether, also in *Dictyostelium*, Nramp1 is involved in metal ion transport in the phago-lysosome, we purified phagosomes in a discontinuous sucrose gradient by adapting a procedure previously used in macrophages (29). As shown in Figure 11, this procedure leads to a phagosomal fraction, which is enriched in markers of the endo-lysosomal pathway, in particular, the membrane proteins VAMP7 (51), Vti1 (51) and vacuolin A (52). Cytosolic markers, such as the actin-binding and adenylyl cyclase-associated protein (CAP) (55) or β-Cop (56), which is associated with vesicles shuttling between endoplasmic recticulum and Golgi, are not found in this fraction. In contrast to β-Cop, the soluble small G-protein Rab7, which associates transiently with endo-lysosomal vesicles, is present but not enriched as the membrane proteins, very likely being washed away during the isolation procedure. Actin, which has been reported to be a heavy contaminant of phagosomal fractions (57), is also found, but not enriched, in our phagosomal preparation (Figure 11).

As antibodies specific for *Dictyostelium* Nramp1 are not yet available, enrichment of Nramp1 in the phagosomal

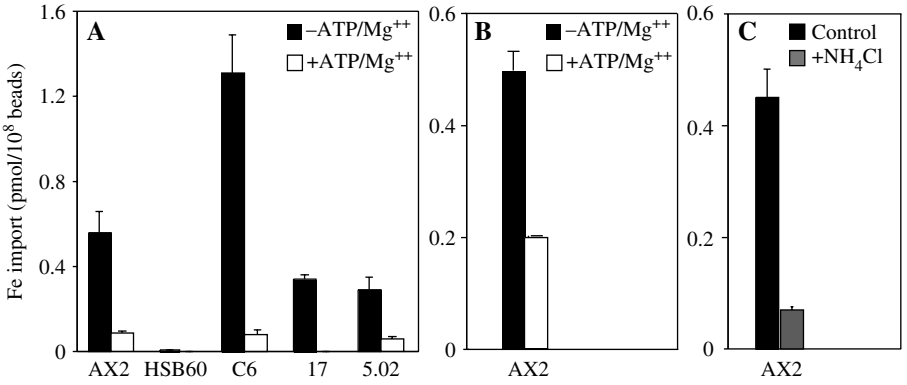

Figure 12: Iron transport in phagosomes purified from different cell lines. (A) Purified phagosomes, containing latex beads, were challenged with 5 μM [^{59}]Fe-citrate in (filled bars) presence or (open bars) absence of 1 mM ATP/2 mM $MgCl_2$ and incubated for 30 min at either 23 °C or on ice, as described in *Materials and Methods*. The reaction was stopped, by adding 10-fold excess of ice-cold iron citrate. The phagosomes were pelleted, washed twice, and the incorporated radioactivity was measured in the β-counter after mixing the pellet with scintillation liquid. The radioactivity bound to phagosomes on ice was similar in the presence or absence of ATP and has been subtracted from the values shown in the graph. Picomoles of incorporated iron were normalized for the number of phagosomes, by measuring light transmission of the latex beads suspensions at 540 nm in a spectrophotometer. C6 is an AX2 clone overexpressing *Nramp1(C)-GFP*. Clones 17 and 5.02 are two rescue clones of mutant HSB60, which have been transfected with *Nramp(C)-GFP* and selected with 20 μg/mL G418. (B) Purified phagosomes of AX2 cells were incubated with 5 μM [^{59}]Fe-citrate for 30 min at 23 °C in the absence of ATP (filled bar) as described in (A), followed by addition of 1 mM ATP/2 mM $MgCl_2$ and further incubation for 30 min (open bar) before washing and measuring the incorporated radioactivity. (C) Purified phagosomes of AX2 cells were preloaded with [^{59}]Fe-citrate in the absence of ATP as described in (B), followed by addition of 15 mM NH4CL for 5 min. The reaction was stopped with excess ice-cold Fe-citrate and the incorporated radioactivity determined. Mean values of three different experiments, each run in triplicate, with SD (error bars) are shown.

fraction was assessed indirectly by immunostaining phagosomes isolated from cells expressing Nramp1(C)-GFP with antibodies against GFP. Also in this case, there is a clear enrichment of Nramp1 in the phagosomal preparation (Figure 11). Although the purification procedure needs further improvement, its efficiency is comparable to other methods used with *Dictyostelium* cells (57), and the yield obtained is optimal for transport studies.

Transport of divalent cations across the phagosomal membrane was assayed by incubating the purified phagosomes with radiolabelled iron citrate. To assess the effect of ATP on iron transport, phagosomes from control, knockout and overexpressing cells were incubated with iron citrate in the presence or absence of ATP, and the amount of incorporated iron measured in the β counter. As shown in Figure 12A, at 23 °C and in the absence of ATP, iron was incorporated, above the background measured at 0 °C, in phagosomes of both AX2 and *Nramp1*-overexpressing cells, not however in *Nramp1*-null cells. In the presence of ATP, iron transport was inhibited both in AX2 and in *Nramp1*-overexpressing cells. To test whether iron transport could be reconstituted in the HSB60 mutant phagosomes by expressing Nramp1(C)-GFP, iron transport was assayed in two transfected cell lines. As shown in Figure 12A, iron transport, corresponding to about 50% of wild-type, was detected in both the clones and was inhibited by ATP. Thus, the GFP chimaera seems to be functional, although we cannot exclude reduced efficiency because of either the tag or the low level of protein expression.

In parallel experiments, phagosomes of AX2 cells were first loaded with iron citrate for 30 min at 23 °C, followed by addition of ATP. ATP addition resulted in iron efflux from the phagosomes (Figure 12B).

Taken together, these results indicate that Nramp1 is required for iron transport across the phago-lysosomal membrane, and they favour the notion that Nramp1 acts by depleting the phago-lysosome of iron if an ATP source is provided. ATP may activate the V-H^+ATPase, thus leading to a proton gradient in the phagosomal lumen that could drive iron export, by coupling it to proton efflux. To test this hypothesis, we preloaded phagosomes with iron and the pH of the medium was then increased of about 1 unit with NH_4Cl. Increasing external pH led to iron export, very likely because of concomitant proton efflux from the phagosomal lumen (Figure 12C).

Discussion

In this article, we have shown that *Dictyostelium* cells express Nramp1, a major determinant of natural resistance to intracellular infections in mice and humans (17). *Dictyostelium* Nramp1 shows a higher homology to mammalian Nramp1 than Nramp2 and is closer to mammalian Nramps than the bacterial or yeast homologues. *Nramp1* gene expression is abruptly downregulated under starving conditions, although the encoded mRNA is present in traces throughout development. Under standard laboratory conditions, development is unaffected in Nramp1-null

mutants, although postaggregative development is accelerated in a few hours. *Dictyostelium* is thus the lowest eukaryotic phagocyte, in which Nramp1 could serve a specific function in bacterial phagocytosis and degradation, suggesting an ancient evolutionary origin of the Nramp1-linked resistance mechanism to pathogens. A second, evolutionary more recent, function of Nramp1 is its involvement in autoimmune diseases (28).

Disrupting *Dictyostelium Nramp1* gene generates cells that are better hosts than wild-type cells for intracellular growth of pathogenic *Mycobacteria* and *Legionella* strains, in agreement with the proposed involvement of Nramp1 in resistance towards invasive bacteria (17,28). Overexpressing *Nramp1* under the control of a constitutive promoter protects efficiently *Dictyostelium* cells from *L. pneumophila,* not however from *M. avium* infection. Rescuing the mutant cells by expressing the GFP construct under the control of the constitutive promoter also resulted in inhibition of *L. pneumophila* cell growth. This intriguing result is not surprising in view of the changes in *Nramp1* gene expression during infection. We have shown that the endogenous *Nramp1* mRNA slowly disappears in the half-starving conditions of the medium used in the infection experiments. *Legionella pneumophila* appears to accelerate this process, whereas *M. avium* displays a rather stimulatory effect on gene accumulation. If *Nramp1* gene expression is inhibited by *Legionella,* the Nramp1 protein will also disappear hours later, making wild-type cells similar to the knockout cell line. If so, expressing *Nramp1(C)-GFP* under the control of the constitutive actin promoter in the knockout background cannot lead to reconstitution of the AX2 phenotype rather of AX2 constitutively expressing *Nramp1*.

Taken together, these results suggest that *Legionella* and *Mycobacteria* use different mechanisms to inactivate Nramp1 activity, probably linked to different requirements for the metal ions and/or different compartmentalization within the host cell.

Nramp1 defines a compartment in the endo-phago-lysosomal pathway

By expressing Nramp1(C)-GFP, comparing its intracellular distribution with GFP-(N)vatB, a subunit of the vacuolar H^+ATPase, and performing immunofluorescence co-labelling with anti-vatA antibodies, we have shown that Nramp1 and V-H^+ATPase identify common and distinct compartments. Nramp1(C)-GFP is located on a subset of acidic vesicles, detectable with neutral red, in addition to non-acidic vacuoles. The latter vesicles are, at least in part, exocytic vesicles, which are positive for vacuolin but negative for GFP-(N)vatB. In resting cells, very few vesicles decorated with the vatA subunit of the vacuolar H^+ATPase are also positive for Nramp1(C)-GFP, suggesting that the two proteins are mostly in separate compartments. Green fluorescent protein-(N)vatB decorates all acidic vesicles and the contractile vacuole system, an osmoregulatory organelle, which is distinct from the endo-phago-lysosomal compartment (43,45,53,58). The interconnected vacuolar tubules and cysternae are free of Nramp1(C)-GFP, which in contrast is found in a distinct perinuclear vesicular cluster not visible in GFP-(N)vatB-expressing cells. The perinuclear cluster is found in all cells, also in very low fluorescent cells, and is duplicated in case of bi-nucleated cells. As evidenced by the GFP chimaeras, in *Dictyostelium*, the cluster is not homogeneous. Most vesicles are very small and highly motile, a few scattered vesicles are acidic, as they co-label with vatA. We suggest that the cluster is coincident with the TGN and vesicles budding from it for the following reasons: (i) the Nramp1(C)-GFP defined perinuclear cluster co-labels with antibodies specific for the Golgi marker comitin; (ii) its location and shape are similar to the Golgi stacks in cells expressing the Golgi marker GFP-golvesin (46) and (iii) most important, the cluster is co-labelled with Vti1. Vti1 is a SNARE component required for transport and docking of vesicles from the *trans*-Golgi to the endosomal pathway (53,54). *Dictyostelium* Vti1 coprecipitate with syntaxin 7, suggesting its association with early endosomal vesicles (52). These findings, and the observation that most vesicles decorated with Vti1 are positive for Nramp1(C)-GFP, raise the possibility that the perinuclear cluster is a *trans*-Golgi and post-Golgi reservoir of the endosomal-recycling compartment. Nramp1 is very likely co-inserted with the Vti1 SNARE complex in the same vesicles in *trans*-Golgi, and this complex regulates fusion of Nramp1-coated vesicles with early endosomes and phagosomes.

Distribution of Nramp1 in vesicles clustered adjacent to the nucleus has also been described in immunofluorescence studies with macrophage cells (32). They have been identified as late endosomes, which in macrophages are located perinuclearly, whereas lysosomes are dispersed throughout the cytoplasm (59).

Taken together, the intracellular compartmentation of V-H^+ATPase and Nramp1, the dynamics of their recruitment during macropinocytosis, the qualitative data on their targeting in yeast and bacterial phagocytosis, indicate that, in *Dictyostelium*, Nramp1 and the vacuolar H^+ATPase reside in different compartments are both absent from nascent endo- and phagosomes but co-associated with macropinocytic and phagocytic vesicles, whether they are immature or whether they have acquired lysosomal characteristics. In the exocytosis pathway, Nramp1 marks an intermediate step, characterized by the co-expression of Nramp1 and vacuolin and the absence of vatB, followed by a final stage in which vacuolin is present but Nramp1 absent.

It is noteworthy that the Nramp1 distribution in the endo-lysosomal pathway, which emerges in *Dictyostelium* using GFP fusion proteins as a tool, strongly resembles what has been found in macrophages using antibodies

against Nramp1 (19,32,60,61). In macrophages, Nramp1 is localized mostly in late endosomes, although some co-fluorescence with early endosomal markers, such as Rab5 and Rab7, was also found (32,60). Upon phagocytosis, Nramp1 is rapidly recruited to the phagosomal membrane and remains associated with many types of immature and mature phagocytic vacuoles (26,60,61).

The high similarity in Nramp1 distribution in *Dictyostelium* and macrophages, using a GFP-fused protein in the first or antibodies in the second case, makes it unlikely that the GFP tag may have led to mislocalization of the fused protein to other compartments. As mentioned, plasma membrane, nucleus, the extended contractile vacuole network as well as nascent endo- and phagosomes are totally free of Nramp1(C)-GFP. In addition, we have shown that the GFP chimaera is functional, if expressed in both AX2 or mutant cells, in which the endogenous gene has been disrupted.

The *in vivo* studies with TRITC-dextran as a tool to follow macropinocytosis suggest that endo- and phagosomes fuse first with vesicles containing vatB, a subunit of the V-H^+ATPase, and shortly thereafter with Nramp1. Yeast particles are suitable for following phagocytosis *in vivo* and have been used in the past by other laboratories and us (1,5). It must be kept in mind, however, that yeasts are large particles that are taken up at a much lower rate than bacteria, and their degree of phagocytosis is subject to high variation from one experiment to the other. Quantitative kinetic studies of phagocytosis need to be done with bacteria or latex beads, and they are in progress in our laboratory. If confirmed with bacteria, our results with TRITC-dextran would in any case suggest that initial acidification is the first barrier invasive bacteria have to cope with. The results on the dynamics of macropinocytosis are in agreement with previous results, which have shown that, in *Dictyostelium*, endosomal acidification starts 1 min after macropinocytosis and within seconds after the endosome looses its protective coat (7). This process is delayed of 1–2 min in case of phagosomes (5). Endosomal acidification increases and persists for 30–40 min, after which the endocytic vesicle becomes neutral and enters the postlysosomal pathway. Undigested material is released 1 h after the beginning of macropinocytosis (7) or even after 2–3 h in the case of latex beads phagocytosis (Bozzaro, unpublished results).

Nramp1 depletes iron from the phago-lysosome in an ATP-dependent process

We have shown that Nramp1 is required for energy-dependent metal ion transport across the phagosomal membrane. If the gene is disrupted, as in HSB60 cells, no iron influx occurs at 23 °C above the background found at 0 °C. Expressing Nramp1 in the mutant background restores iron influx. The directionality of iron transport across the phagosomal membrane is however dependent on ATP. If an ATP source is provided, iron influx is inhibited and iron efflux from the phagosome favoured. Altering the proton gradient with ammonium chloride also leads to efflux of preloaded iron. Caution is required in interpreting these results, as direct evidence that Nramp1 mediates both metal cation influx and efflux is still lacking. Our results do not exclude the possibility that Nramp1 may be involved solely in metal cation influx and that the ATP-dependent iron efflux is mediated by a different transporter. If we assume that Nramp1 is the major or only metal cation transporter involved in the process, the present results would indicate that Nramp1 acts as a symporter of protons and metal cations in an ATP-dependent process.

These results may help explaining a long-debated question on Nramp1 mechanism of action in macrophages. *In vivo* assays with a divalent cation-sensitive and pH-resistant fluorophore, chemically coupled to zymosan, have led Gros and coworkers (17,26,62) to propose that Nramp1 functions as a pH-dependent and bafilomycin-sensitive divalent cation efflux pump. Import studies with isolated phagosomes have instead led to the conclusion that Nramp1 transports iron into the phagosome (27,63). However, in the latter studies with isolated phagosomes, no ATP was added to the phagosomal suspension during iron uptake. Our results with isolated phagosomes clearly show that the directionality of iron flux is affected by ATP. In its absence, a net iron influx is found also in *Dictyostelium* phagosomes, whereas influx is strongly reduced in the presence of ATP. ATP also induces efflux of previously loaded iron. We propose that ATP is required for activating the V-H^+ATPase, leading to proton influx in the phago-lysosome. Proton efflux through Nramp1 would then be required for symport activity of Nramp1, thus depleting the phago-lysosome of iron. The *in vivo* activity of Nramp1 will therefore depend on whether or not the protein co-localizes with the V-H^+ATPase. If we assume that the non-acidic, Nramp1-positive vesicles are mostly in the postlysosomal pathway, then Nramp1 activity during microbial infection would be mainly regulated by the V-H^+ATPase, thus resulting in phagosomal depletion of iron and other metal ions, which are essential for bacterial growth, as suggested in their original hypothesis by Gros and coworkers (26).

Different scenarios can be envisaged for pathogenic bacteria, which might either inhibit phagosomal fusion with Nramp1-positive vesicles or block their acidification, thus neutralizing or even exploiting Nramp1 to their advantage and/or inhibit Nramp1 expression. In the case of *M. avium*, we have shown that (i) its growth rate is higher in Nramp1-null compared with wild-type cells, (ii) overexpressing Nramp1 in the wild-type background has no additional protective effect and (iii) *Nramp1* gene expression is not inhibited rather stimulated during infection. Reduced fusion to lysosomes increased retention of endosomal markers, and a rather neutral environment has been

described in macrophage phagosomes containing living *Mycobacteria* (60,64,65), probably as a result of reduced density of V-H^+ATPases at the phagosomal membrane (65,66). Interestingly, a positive effect of *Mycobacteria* on *Nramp1* gene expression has also been reported in macrophages (67). Thus, *Mycobacteria* appear to grow better in the absence of Nramp1 but can also exploit Nramp1 to their advantage. It is conceivable that, at neutral pH, Nramp1 is used by *Mycobacteria* to scavenge iron required for their intraphagosomal growth as suggested by Forbes and Gros (17). Experiments are underway to test this hypothesis.

Unlike *M. avium*, *L. pneumophila* proliferates much better in Nramp1-null than wild-type cells and probably inhibits in the long-run *Nramp1* gene expression. We conclude that *L. pneumophila* avoids rather than exploiting the Nramp1 environment, possibly because of different growth requirements than *M. avium*. Consistent with this hypothesis, *L. pneumophila* intracellular growth is efficiently antagonized by *Nramp1* overexpression in the host cell. In macrophages, it has been shown that, following internalization, *Legionella* manipulates the host endo-lysosomal degradation pathway to survive and to replicate in a vacuole, which is derived from the endoplasmic reticulum (68,69). Evidence has been recently provided that this holds true also for *Dictyostelium* (37). Interestingly, in macrophages and monocytes, *L. pneumophila* delays but does not abolish the acidification process, and after 18 h from infection, the bacteria reside and proliferate in an acidic compartment, although acidification is not a prerequisite for growth (70,71). If acidification is not abolished, Nramp1 neutralization can be better accomplished by inhibiting its mRNA expression, which in *Dictyostelium* would result in disappearance of the protein within few hours. We have found no data in the literature concerning effects of *L. pneumophila* infection on mammalian *Nramp1* gene expression. The present results are thus the first report on this possible mechanism, which may be used by *L. pneumophila* also in macrophages.

The present results establish *Dictyostelium* as an excellent host model, complementary to macrophages, for studying the mechanism of action of Nramp1 and its role in bacterial infections. Studies are underway to test to which extent *M. avium* and *L. pneumophila* affect phagosomal fusion with Nramp1-positive vesicles, and whether this process, the outcome of infection and *Nramp1* gene expression are altered by metal ions.

Materials and Methods

Cell cultures

Dictyostelium discoideum wild-type strain AX2, *Nramp1* knockout mutant HSB60 and all other cell lines were grown axenically in AX2 medium (72), under shaking at 150 r.p.m and 23 °C. Blasticidin at a concentration of 10 μg/mL was added to Nramp1-null mutant cell cultures. Cells expressing proteins fused with GFP were cultured in presence of 10, 20 or 60 μg/mL G418. No differences, except for fluorescence intensity, were found in intracellular distribution of the fluorescent protein in cells with lower or higher selection. For starvation, cells were washed twice in 0.017 M Na-K Soerensen phosphate buffer, pH 6.0, and shaken in the same buffer at the concentration of 10^7 per mL (73).

C6 is an AX2 clone overexpressing *Nramp1(C)-GFP* and clones 5.02 and 17 are two independent rescue clones obtained by transfecting *Nramp1(C)-GFP* in the HSB60 background, followed by selection with 20 μg/mL G-418.

Antibodies

For immunoblotting and/or immunofluorescence, the following antibodies were used: rabbit polyclonal antibodies against LmpA (74), Rab7 (75) and against cytoplasmic fragments of Vti1 and VAMP7 (51); mouse monoclonal antibodies against the vatA subunit of V-H^+ATPase (76), vacuolin A (48), comitin (47), Cap (55), GFP (37) and actin (77).

Growth, phagocytosis and infection assays

Cell growth in shaken *E. coli* bacterial suspension or on bacterial lawn and phagocytosis of fluorescein isothiocyanate-labelled bacteria was measured as described (5). Infection and intracellular growth of *L. pneumophila* Corby or *M. avium* were done as described (34,35,38).

Purification of Dictyostelium phagosomes

Phagosomes were purified by adapting to *Dictyostelium* cells a procedure established for macrophages (27,29). Briefly, a total of 4×10^8 *Dictyostelium* cells were mixed with 1-μm latex beads (Fluoresbrite™ carboxy NYO microspheres, Polysciences Inc., Eppelsheim, Germany), at a ratio of 1:100 in a volume of 50 mL and incubated for 30 min at 23 °C under shaking. Cells were washed twice by centrifugation at 120 × ***g*** and resuspended in 2 mL of ice-cold homogenization buffer (50 mM Tris-HCl, pH 7,5; 250 mM sucrose; 1 mM ethylenediaminetetraacetic acid; 1 mM phenylmethylsulphonyl fluoride; 1 mM Na_3VO_4). Cells were lysed by filtering through a 3-μm polycarbonate filter (Ge Osmonics Labstore, Minnetonga, MN, USA). The resulting homogenate was diluted 1:3 with Soerensen phosphate buffer and centrifuged for 5 min at 150 × ***g*** to remove unbroken cells and large debris. The supernatant was filtered through a 5-μm Nucleopore filter (Corning, Acton, MA, USA). The filter was rinsed with 1.5 mL of Soerensen phosphate buffer, and the rinse was added to the original filtrate. The solution was layered on top of a discontinuous sucrose gradient, consisting of 3 mL of 12% sucrose on top of 1 mL 50% sucrose cushion (in 20 mM Tris-HCl pH 7,5), and centrifuged at 800 × ***g*** for 1 h at 4 °C. The phagosomes, evident as a pink band, were recovered from the 12–50% sucrose interface, diluted threefold with Soerensen phosphate buffer and placed on top of a 2-mL cushion (12% Ficoll in 20 mM TRIS-HCl, pH 7.5). The solution was centrifuged at 800 × ***g*** for 60 min at 4 °C, and the pellet was resuspended in Soerensen phosphate buffer and used for iron uptake experiments.

In vitro iron import into phagosomal vesicles

Iron import was started by adding an equal volume of fivefold diluted import substrate solution (20 mM Hepes/Tris pH 6; 30 mM HCl; 5 mM sodium citrate; 50 μM [^{59}Fe] ferric chloride) to 50 μL of phagosomal vesicles in 1.5 mL centrifuge tubes (29). The final pH in the mixture is between 5 and 5.5 (measured with pH-indicator strips). The experiments were done in the absence or presence of 1 mM ATP/2 mM $MgCl_2$. After 30 min incubation at 4 °C or 23 °C, the import reaction was terminated by adding 0.5 mL of ice-cold Fe-citrate (0.5 μM in 20 mM TRIS-HCl, pH 7.5). Phagosomes were washed twice from unincorporated [^{59}]Fe-citrate by centrifugation at 16 000 × g for 4 min at 4 °C with Soerensen phosphate buffer. The radioactivity was measured in the β-counter after mixing the pellet with scintillation liquid. In some experiments, phagosomes were first loaded with iron for 30 min before adding ATP for additional 30 min. Preloaded phagosomes were also treated with 15 mM NH_4Cl for 5 min before stopping the reaction with ice-cold Fe-citrate.

Gene cloning and sequencing

Genomic DNA from growing AX2 cells was prepared as described by Sambrook *et al.* (78). Genomic DNA or cDNA were amplified with appropriate primers and cloned in either pGEM-T or pGEM-TEasy (Promega, Madison, WI, USA) according to Sambrook *et al.* (78). DNA clones were sequenced with gene-specific primers using automated sequencers (ABI 3700, Perkin Elmer, Norwalk, CT, USA or ALF Express II, Amersham-Pharmacia Biotech, Uppsala, Sweden). For sequence analysis, the GCG and ALFWIN 2.0 package softwares were used. Homologous sequences and sequence tags were routinely searched through the National Centre for Biotechnology Information or the *Dictyostelium* Genome Imb-Jena databases with the BLAST or FAST servers. For sequence alignments and protein predictions, the MACVECTOR 7.0 software package was used.

Vector construction and cell transformation

For expression of fusion proteins with GFP, the pDEX-GFPN (79) and pDEX-GFPC vectors (Westphal, unpublished), both containing the constitutive *actin-15* promoter, were used. To express GFP-(N)vatB, the *vatB*-coding sequence was amplified from the pGEM-T-vatB vector (39) with two specific primers containing a *Cla I* site and inserted into the *Cla I* site of the pDEX-GFPN vector with (N)vatB connected to S65T-GFP by the linker KLEFID. To express Nramp1(C)-GFP, the *Nramp1*-coding sequence was amplified from the pGEM-TEasy-*Nramp1* with two specific primers containing an *EcoR I* site and inserted into the *EcoR I* site of the pDEX-GFPC vector with Nramp1(C) connected to S65T-GFP by the linker EFKKLK.

Cell transformation was done by electroporation (80), and transformants were selected on plates in nutrient medium containing 10 μg/mL G418. In some cell lines expressing GFP-fusion proteins, the G418 concentration was gradually increased to 60 μg/mL to improve fluorescence intensity.

Construction of Nramp1 knockout strains

The *bsr*, used as selectable marker, was excised from pUCBsrΔBam (81) with *Hind* III and *Xba* I. The *bsr* cassette was ligated, using the 'DNA ligation kit' (Amersham Biosciences Europe, Cologno Monzese, Italy), in the opposite direction into the unique *Cla I* site of the 1350 bp *Nramp1* sequence downstream the intron region. The vector, carrying the selectable marker, was linearized with *Sph I* and *Sal I* and electroporated into the parental strain (80). The transformed cell population was splitted in 96-well plates and grown in the presence of 10 μg/mL of blasticidin. Resistant colonies were subcloned and screened in Southern blots to identify clones, in which the *Nramp1* gene was disrupted. Three independent clones were isolated and further studied.

In vivo microscopy and fluorescence imaging

Incubation of living cells expressing Nramp1(C)-GFP or GFP-(N)vatB with yeast particles or TRITC-dextran was done as described (5,46). Pulse-chase experiments with TRITC-dextran (Molecular Probes, Eugene, OR, USA) were done by incubating the cells with 1 mg/mL TRITC-dextran for 5 min in suspension, washing and plating the cells on a 6 × 6 cm glass coverslip equipped with a 5-cm diameter Plexiglas ring, subjected or not to agar overlay (45). For staining acidic vesicles, cells were incubated with 0.1 μM neutral red (Sigma, St Louis, MO, USA). Confocal serial images were taken on an inverted Zeiss LSM510 microscope as described (5), except that the scanning interval was reduced to 7.2 seconds.

Northern and Southern blotting

Total RNA was isolated using the TRIzol reagent (Invitrogen, Carlsbad, CA, USA), according to the manufacturer's instructions. RNA electrophoresis on denaturing-agarose-formaldehyde gels and Northern and Southern blot analysis were done as described (39,78).

SDS–PAGE and immunoblotting

Proteins from total cell lysate or purified phagosomes were separated by electrophoresis in 10% polyacrylamide gels with SDS, blotted onto nitrocellulose and incubated with antibodies as previously described (73). For Western blots, horseradish peroxidase-coupled goat anti-mouse (Amersham Biotech) or anti-rabbit immunoglobulin G (Santa Cruz Biotechnologies, Santa Cruz, CA, USA) were used at a dilution of 1:10.000 and revealed by chemiluminescence, using Pierce (Rockford, IL, USA) Supersignal, according to the manufacturer's instructions.

Immunofluorescence labelling

For immunofluorescence studies, cells were fixed with cold methanol, incubated with antibodies and mounted with Gelvatol as described (5). As second antibody, TRITC-labelled rabbit anti-mouse or goat anti-rabbit IgGs (Jackson ImmunoResearch, West Grove, PA, USA) at a final concentration of 0.03 mg/mL were used.

Acknowledgments

We thank M. Westphal and G. Gerisch for the pDEX-GFP vectors, M. Maniak for anti-vacuolin and anti-vatA, M. Schleicher for anti-lmpA antibodies, N. Bennet and F. Bruckert for antibodies against Rab7, VAMP1 and Vti1. We are grateful to the Genome Sequencing Consortium for sequencing the *Dictyostelium* genome and for DNA clones. Without their work, cloning the entire *Nramp1* gene would have required much longer time. The work was supported by funds of the Italian Ministry for University and Research (PRIN'01–'04) and of the Piemonte Region (RSF and RSA'03) to S. Bozzaro and of the DFG (STE 838/3–3) to M. Steinert.

References

1. Maniak M, Rauchenberger R, Albrecht R, Murphy J, Gerisch G. Coronin involved in phagocytosis: dynamics of particle-induced relocalization visualized by a green fluorescent protein tag. Cell 1995;83: 915–924.
2. Bracco E, Pergolizzi B, Peracino B, Ponte E, Balbo A, Mai A, Ceccarelli A, Bozzaro S. Cell-cell signaling and adhesion in phagocytosis and early development of *Dictyostelium*. Int J Dev Biol 2000;44:733–742.
3. Duhon D, Cardelli J. The regulation of phagosome maturation in *Dictyostelium*. J Muscle Res Cell Motil 2002;23:803–808.
4. Greenberg S. Signal transduction of phagocytosis. Trends Cell Biol 1995;5:93–99.
5. Peracino B, Borleis J, Jin T, Westphal M, Schwartz JM, Wu L, Bracco E, Gerisch G, Devreotes P, Bozzaro S. G protein beta subunit-null mutants are impaired in phagocytosis and chemotaxis due to inappropriate regulation of the actin cytoskeleton. J Cell Biol 1998;141: 1529–1537.
6. May RC, Machesky LM. Phagocytosis and the actin cytoskeleton. J Cell Sci 2001;114:1061–1077.
7. Maniak M. Organelle transport: a park-and-ride system for melanosomes. Curr Biol 2003;13:R917–R919.
8. Jahraus A, Tjelle TE, Berg T, Habermann A, Storrie B, Ullrich O, Griffiths G. In vitro fusion of phagosomes with different endocytic organelles from J774 macrophages. J Biol Chem 1998;273: 30379–30390.
9. Rupper A, Grove B, Cardelli J. Rab7 regulates phagosome maturation in *Dictyostelium*. J Cell Sci 2001;114:2449–2460.
10. Cox D, Greenberg S. Phagocytic signaling strategies: Fc (gamma) receptor-mediated phagocytosis as a model system. Semin Immunol 2001;13:339–345.
11. Garin J, Diez R, Kieffer S, Dermine JF, Duclos S, Gagnon E, Sadoul R, Rondeau C, Desjardins M. The phagosome proteome: insight into phagosome functions. J Cell Biol 2001;152:165–180.

12. Cardelli J. Phagocytosis and macropinocytosis in *Dictyostelium:* phosphoinositide-based processes, biochemically distinct. Traffic 2001;2:311–320.
13. Eichinger L, Pachebat JA, Glockner G, Rajandream MA, Sucgang R, Berriman M, Song J, Olsen R, Szafranski K, Xu Q, Tunggal B, Kummerfeld S, Madera M, Konfortov BA, Rivero F *et al.* The genome of the social amoeba *Dictyostelium discoideum*. Nature 2005;435: 43–57.
14. Eichinger L, Noegel AA. Crawling into a new era-the *Dictyostelium* genome project. Embo J 2003;22:1941–1946.
15. Vidal SM, Malo D, Vogan K, Skamene E, Gros P. Natural resistance to infection with intracellular parasites: isolation of a candidate for Bcg. Cell 1993;73:469–485.
16. Barton CH, Whitehead SH, Blackwell JM. Nramp transfection transfers Ity/Lsh/Bcg-related pleiotropic effects on macrophage activation: influence on oxidative burst and nitric oxide pathways. Mol Med 1995;1:267–279.
17. Forbes JR, Gros P. Divalent-metal transport by NRAMP proteins at the interface of host–pathogen interactions. Trends Microbiol 2001;9: 397–403.
18. Vidal SM, Pinner E, Lepage P, Gauthier S, Gros P. Natural resistance to intracellular infections: Nramp1 encodes a membrane phosphoglycoprotein absent in macrophages from susceptible (Nramp1, D169) mouse strains. J Immunol 1996;157:3559–3568.
19. White JK, Stewart A, Popoff JF, Wilson S, Blackwell JM. Incomplete glycosylation and defective intracellular targeting of mutant solute carrier family 11 member 1 (Slc11a1). Biochem J 2004;382:811–819.
20. Blackwell JM, Searle S, Mohamed H, White JK. Divalent cation transport and susceptibility to infectious and autoimmune disease: continuation of the Ity/Lsh/Bcg/Nramp1/Slc11a1 gene story. Immunol Lett 2003;85:197–203.
21. Wyllie S, Seu P, Goss JA. The natural resistance-associated macrophage protein 1 Slc11a1 (formerly Nramp1) and iron metabolism in macrophages. Microbes Infect 2002;4:351–359.
22. Gruenheid S, Cellier M, Vidal S, Gros P. Identification and characterization of a second mouse Nramp gene. Genomics 1995;25:514–525.
23. Supek F, Supekova L, Nelson H, Nelson N. A yeast manganese transporter related to the macrophage protein involved in conferring resistance to mycobacteria. Proc Natl Acad Sci USA 1996;93:5105–5110.
24. Gunshin H, Mackenzie B, Berger UV, Gunshin Y, Romero MF, Boron WF, Nussberger S, Gollan JL, Hediger MA. Cloning and characterization of a mammalian proton-coupled metal-ion transporter. Nature 1997;388:482–488.
25. Atkinson PG, Barton CH. Ectopic expression of Nramp1 in COS-1 cells modulates iron accumulation. FEBS Lett 1998;425:239–242.
26. Jabado N, Jankowski A, Dougaparsad S, Picard V, Grinstein S, Gros P. Natural resistance to intracellular infections: natural resistance-associated macrophage protein 1 (Nramp1) functions as a pH-dependent manganese transporter at the phagosomal membrane. J Exp Med 2000;192:1237–1248.
27. Zwilling BS, Kuhn DE, Wikoff L, Brown D, Lafuse W. Role of iron in Nramp1-mediated inhibition of mycobacterial growth. Infect Immun 1999;67:1386–1392.
28. Blackwell JM, Searle S, Goswami T, Miller EN. Understanding the multiple functions of Nramp1. Microbes Infect 2000;2:317–321.
29. Kuhn DE, Lafuse WP, Zwilling BS. Iron transport into mycobacterium avium-containing phagosomes from an Nramp1 (Gly169)-transfected RAW264.7 macrophage cell line. J Leukoc Biol 2001;69:43–49.
30. de Chastellier C, Frehel C, Offredo C, Skamene E. Implication of phagosome-lysosome fusion in restriction of *Mycobacterium avium* growth in bone marrow macrophages from genetically resistant mice. Infect Immun 1993;61:3775–3784.
31. Hackam DJ, Rotstein OD, Zhang W, Gruenheid S, Gros P, Grinstein S. Host resistance to intracellular infection: mutation of natural resistance-associated macrophage protein 1 (Nramp1) impairs phagosomal acidification. J Exp Med 1998;188:351–364.
32. Searle S, Bright NA, Roach TI, Atkinson PG, Barton CH, Meloen RH, Blackwell JM. Localisation of Nramp1 in macrophages: modulation with activation and infection. J Cell Sci 1998;111:2855–2866.
33. Depraitere C, Darmon M. [Growth of '*Dictyostelium discoideum*' on different species of bacteria (author's transl)]. Ann Microbiol (Paris) 1978;129B:451–461.
34. Skriwan C, Fajardo M, Hägele S, Horn M, Wagner M, Michel R, Krohne G, Schleicher M, Hacker J, Steinert M. Various bacterial pathogens and symbionts infect the amoeba *Dictyostelium discoideum*. Int J Med Microbiol 2002;291:615–624.
35. Hägele S, Kohler R, Merkert H, Schleicher M, Hacker J, Steinert M. *Dictyostelium discoideum*: a new host model system for intracellular pathogens of the genus Legionella. Cell Microbiol 2000;2:165–171.
36. Solomon JM, Rupper A, Cardelli JA, Isberg RR. Intracellular growth of *Legionella pneumophila* in *Dictyostelium discoideum*, a system for genetic analysis of host-pathogen interactions. Infect Immun 2000;68:2939–2947.
37. Fajardo M, Schleicher M, Noegel A, Bozzaro S, Killinger S, Heuner K, Hacker J, Steinert M. Calnexin, calreticulin and cytoskeleton-associated proteins modulate uptake and growth of *Legionella pneumophila* in *Dictyostelium discoideum*. Microbiology 2004;150: 2825–2835.
38. Otto GP, Wu MY, Kazgan N, Anderson OR, Kessin RH. *Dictyostelium* macroautophagy mutants vary in the severity of their developmental defects. J Biol Chem 2004;279:15621–15629.
39. Bracco E, Peracino B, Noegel AA, Bozzaro S. Cloning and transcriptional regulation of the gene encoding the vacuolar/H^+ ATPase B subunit of *Dictyostelium discoideum*. FEBS Lett 1997;419:37–40.
40. Cellier M, Prive G, Belouchi A, Kwan T, Rodrigues V, Chia W, Gros P. Nramp defines a family of membrane proteins. Proc Natl Acad Sci USA 1995;92:10089–10093.
41. Loomis WF, Smith DW. Molecular phylogeny of *Dictyostelium discoideum* by protein sequence comparison. Proc Natl Acad Sci USA 1990;87:9093–9097.
42. Baldauf SL, Roger AJ, Wenk-Siefert I, Doolittle WF. A kingdom-level phylogeny of eukaryotes based on combined protein data. Science 2000;290:972–977.
43. Heuser J, Zhu Q, Clarke M. Proton pumps populate the contractile vacuoles of *Dictyostelium* amoebae. J Cell Biol 1993;121:1311–1327.
44. Moniakis J, Coukell MB, Janiec A. Involvement of the Ca^{2+}-ATPase PAT1 and the contractile vacuole in calcium regulation in *Dictyostelium discoideum*. J Cell Sci 1999;112:405–414.
45. Gabriel D, Hacker U, Kohler J, Müller-Taubenberger A, Schwartz JM, Westphal M, Gerisch G. The contractile vacuole network of *Dictyostelium* as a distinct organelle: its dynamics visualized by a GFP marker protein. J Cell Sci 1999;11:3995–4005.
46. Schneider N, Schwartz JM, Kohler J, Becker M, Schwarz H, Gerisch G. Golvesin-GFP fusions as distinct markers for Golgi and post-Golgi vesicles in *Dictyostelium* cells. Biol Cell 2000;92:495–511.
47. Weiner OH, Murphy J, Griffiths G, Schleicher M, Noegel AA. The actin-binding protein comitin (p24) is a component of the Golgi apparatus. J Cell Biol 1993;123:23–34.
48. Jenne N, Rauchenberger R, Hacker U, Kast T, Maniak M. Targeted gene disruption reveals a role for vacuolin B in the late endocytic pathway and exocytosis. J Cell Sci 1998;111:61–70.
49. Fischer von Mollard G, Stevens TH. The *Saccharomyces cerevisiae* v-SNARE Vti1p is required for multiple membrane transport pathways to the vacuole. Mol Biol Cell 1999;10:1719–1732.
50. Chidambaram S, Mullers N, Wiederhold K, Haucke V, von Mollard GF. Specific interaction between SNAREs and epsin N-terminal homology (ENTH) domains of epsin-related proteins in trans-Golgi network to endosome transport. J Biol Chem 2004;279:4175–4179.

51. Bogdanovic A, Bennett N, Kieffer S, Louwagie M, Morio T, Garin J, Satre M, Bruckert F. Syntaxin 7, syntaxin 8, Vti1 and VAMP7 (vesicle-associated membrane protein 7) form an active SNARE complex for early macropinocytic compartment fusion in *Dictyostelium discoideum*. Biochem J 2002;368:29–39.
52. Rauchenberger R, Hacker U, Murphy J, Niewohner J, Maniak M. Coronin and vacuolin identify consecutive stages of a late, actin-coated endocytic compartment in *Dictyostelium*. Curr Biol 1997;7:215–218.
53. Clarke M, Kohler J, Arana Q, Liu T, Heuser J, Gerisch G. Dynamics of the vacuolar H(+)-ATPase in the contractile vacuole complex and the endosomal pathway of *Dictyostelium* cells. J Cell Sci 2002;115:2893–2905.
54. Giglione C, Gross JD. Anion effects on vesicle acidification in *Dictyostelium*. Biochem Mol Biol Int 1995;36:1057–1065.
55. Gottwald U, Brokamp R, Karakesisoglou I, Schleicher M, Noegel AA. Identification of a cyclase-associated protein (CAP) homologue in *Dictyostelium discoideum* and characterization of its interaction with actin. Mol Biol Cell 1996;7:261–272.
56. Mohrs MR, Janssen KP, Kreis T, Noegel AA, Schleicher M. Cloning and characterization of beta-COP from *Dictyostelium discoideum*. Eur J Cell Biol 2000;79:350–357.
57. Gotthardt D, Warnatz HJ, Henschel O, Bruckert F, Schleicher M, Soldati T. High-resolution dissection of phagosome maturation reveals distinct membrane trafficking phases. Mol Biol Cell 2002;13:3508–3520.
58. Temesvari LA, Bush JM, Peterson MD, Novak KD, Titus MA, Cardelli JA. Examination of the endosomal and lysosomal pathways in *Dictyostelium discoideum* myosin I mutants. J Cell Sci 1996;109:663–673.
59. Griffiths G, Hoflack B, Simons K, Mellman I, Kornfeld S. The mannose 6-phosphate receptor and the biogenesis of lysosomes. Cell 1988;52:329–341.
60. Gruenheid S, Pinner E, Desjardins M, Gros P. Natural resistance to infection with intracellular pathogens: the Nramp1 protein is recruited to the membrane of the phagosome. J Exp Med 1997;185:717–730.
61. Frehel C, Canonne-Hergaux F, Gros P, De Chastellier C. Effect of Nramp1 on bacterial replication and on maturation of *Mycobacterium avium*-containing phagosomes in bone marrow-derived mouse macrophages. Cell Microbiol 2002;4:541–556.
62. Forbes JR, Gros P. Iron, manganese, and cobalt transport by Nramp1 (Slc11a1) and Nramp2 (Slc11a2) expressed at the plasma membrane. Blood 2003;102:1884–1892.
63. Kuhn DE, Baker BD, Lafuse WP, Zwilling BS. Differential iron transport into phagosomes isolated from the RAW264.7 macrophage cell lines transfected with Nramp1Gly169 or Nramp1Asp169. J Leukoc Biol 1999;66:113–119.
64. de Chastellier C, Lang T, Thilo L. Phagocytic processing of the macrophage endoparasite, *Mycobacterium avium,* in comparison to phagosomes which contain Bacillus subtilis or latex beads. Eur J Cell Biol 1995;68:167–182.
65. Hackam DJ, Rotstein OD, Zhang WJ, Demaurex N, Woodside M, Tsai O, Grinstein S. Regulation of phagosomal acidification. Differential targeting of Na^+/H^+ exchangers, Na^+/K^+-ATPases, and vacuolar-type H^+-ATPases. J Biol Chem 1997;272:29810–29820.
66. Schaible UE, Sturgill-Koszycki S, Schlesinger PH, Russell DG. Cytokine activation leads to acidification and increases maturation of *Mycobacterium avium*-containing phagosomes in murine macrophages. J Immunol 1998;160:1290–1296.
67. Zhong W, Lafuse WP, Zwilling BS. Infection with *Mycobacterium avium* differentially regulates the expression of iron transport protein mRNA in murine peritoneal macrophages. Infect Immun 2001;69:6618–6624.
68. Swanson MS, Isberg RR. Association of *Legionella pneumophila* with the macrophage endoplasmic reticulum. Infect Immun 1995;63:3609–3620.
69. Roy CR. Exploitation of the endoplasmic reticulum by bacterial pathogens. Trends Microbiol 2002;10:418–424.
70. Sturgill-Koszycki S, Swanson MS. *Legionella pneumophila* replication vacuoles mature into acidic, endocytic organelles. J Exp Med 2000;192:1261–1272.
71. Wieland H, Goetz F, Neumeister B. Phagosomal acidification is not a prerequisite for intracellular multiplication of *Legionella pneumophila* in human monocytes. J Infect Dis 2004;189:1610–1614.
72. Watts DJ, Ashworth JM. Growth of myxameobae of the cellular slime mould *Dictyostelium discoideum* in axenic culture. Biochem J 1970;119:171–174.
73. Bozzaro S, Merkl R, Gerisch G. Cell adhesion: its quantification, assay of the molecules involved, and selection of defective mutants in *Dictyostelium* and *Polysphondylium*. Methods Cell Biol 1987;28: 359–385.
74. Karakesisoglou I, Janssen KP, Eichinger L, Noegel AA, Schleicher M. Identification of a suppressor of the *Dictyostelium* profilin-minus phenotype as a CD36/LIMP-II homologue. J Cell Biol 1999;145:167–181.
75. Laurent O, Bruckert F, Adessi C, Satre M. In vitro reconstituted *Dictyostelium discoideum* early endosome fusion is regulated by Rab7 but proceeds in the absence of ATP-Mg^{2+} from the bulk solution. J Biol Chem 1998;273:793–799.
76. Fok AK, Clarke M, Ma L, Allen RD. Vacuolar H(+)-ATPase of *Dictyostelium discoideum*. A monoclonal antibody study. J Cell Sci 1993;106:1103–1113.
77. Simpson PA, Spudich JA, Parham P. Monoclonal antibodies prepared against *Dictyostelium* actin: characterization and interactions with actin. J Cell Biol 1984;99:287–295.
78. Sambrook J, Maniatis T, Fritsch EF. Molecular Cloning: A Laboratory Manual, 2nd edn. Cold Spring Harbor, NY: Cold Spring Harbor Laboratory;1989.
79. Westphal M, Jungbluth A, Heidecker M, Muhlbauer B, Heizer C, Schwartz JM, Marriott G, Gerisch G. Microfilament dynamics during cell movement and chemotaxis monitored using a GFP-actin fusion protein. Curr Biol 1997;7:176–183.
80. Pang KM, Lynes MA, Knecht DA. Variables controlling the expression level of exogenous genes in *Dictyostelium*. Plasmid 1999;41:187–197.
81. Adachi H, Hasebe T, Yoshinaga K, Ohta T, Sutoh K. Isolation of *Dictyostelium discoideum* cytokinesis mutants by restriction enzyme-mediated integration of the blasticidin S resistance marker. Biochem Biophys Res Commun 1994;205:1808–1814.